Virology from the perspective of theoretical colloid and interface science

Available online at www.sciencedirect.com

ScienceDirect

Current Opinion in
Colloid & Interface Science

Virology from the perspective of theoretical colloid and interface science

Vladimir P. Zhdanov[1,2]

Abstract

Viral infections occur at very different length and time scales and include various processes, which can often be described using the models developed and/or employed in colloid and interface science. Bearing in mind the currently active COVID-19, I discuss herein the models aimed at viral transmission via respiratory droplets and the contact of virions with the epithelium. In a more general context, I outline the models focused on penetration of virions via the cellular membrane, initial stage of viral genome replication, and formation of viral capsids in cells. In addition, the models related to a new generation of drug delivery vehicles, for example, lipid nanoparticles with size about 100–200 nm, are discussed as well. Despite the high current interest in all these processes, their understanding is still limited, and this area is open for new theoretical studies.

Addresses

[1] Section of Nano and Biological Physics, Department of Physics, Chalmers University of Technology, Göteborg, Sweden
[2] Boreskov Institute of Catalysis, Russian Academy of Sciences, Novosibirsk, Russia

Corresponding author: Zhdanov, Vladimir P (zhdanov@catalysis.ru)

Current Opinion in Colloid & Interface Science 2021, **53**:101450

This review comes from a themed issue on **Hot Topic: COVID-19**

Edited by **Reinhard Miller** and **Libero Liggieri**

For a complete overview see the Issue and the Editorial

https://doi.org/10.1016/j.cocis.2021.101450

Keywords

Virions, Nanoparticles, Respiratory droplets, Diffusion, Association, Dissociation.

Introduction

The scope of the colloid and interface science (CIS) is extremely wide. According to the current instruction for authors of the Journal of CIS, for example, it includes (i) colloidal materials and nanomaterials; (ii) soft colloidal and self-assembly systems; (iii) adsorption, catalysis, and electrochemistry; (iv) interfacial processes, capillarity, and wetting; (v) biomaterials and nanomedicine; and (vi) energy conversion and storage, and environmental technologies. Looking through this list, one can notice that items (i)–(v) are related to biology in general and virology and pharmaceutics in particular. Practically, this means that the basic concepts, experimental techniques, and theoretical models developed in CIS can often be used in virology to scrutinize the elementary processes occurring during transmission of viral infections and function of viruses inside hosts and to optimize and/or find the ways of fighting with viral infections.

Compared to CIS, the scope of virology might appear to be much narrower at first sight. In fact, however, the latter scope is very wide as well, because viral infections occur at very different length and time scales and, because of the diversity of viruses, include a multitude of processes with complex mechanistic details [1]. Basically, viruses are biological nanoparticles (virions) of spherical (with a diameter ranging typically from 60 to 200 nm) or other shapes. Their DNA or RNA genome is protected by a protein capsid and sometimes also by a lipid membrane envelope. At the coarse-grained level, viral infection is reduced to transmission and intracellular replication of virions. The ways of transmission are diverse. The viral replication cycle includes virion attachment to a host-cell lipid membrane, penetration, uncoating and release of genome, genome replication, viral protein synthesis, capsid assembly, and escape from the host. The understanding of all these steps is still rather limited.

Historically, CIS was always based on the general physicochemical concepts and theoretical models. One of the famous generic examples is Smoluchowski's seminal model of diffusion-limited coagulation of colloidal particles. Another famous example is the Derjaguin–Landau–Verwey–Overbeek theory of interaction between colloids. Both these approaches are widely used in various fields of natural sciences already many decades. Nowadays, CIS includes many other models, which can be employed in biology in general and virology in particular. Some of these recently proposed models are discussed below partially with emphasis on the currently active coronavirus disease 2019 (COVID-19).

Viral transmission

At the lumped level, the viral transmission occurs horizontally from host to host or vertically from one

generation of hosts to the next [1]. More specifically, the human viruses are transmitted via (i) disruptions of the skin, (ii) mucosal membranes of the eye and genitourinary tract, (iii) alimentary canal, and (iv) respiratory tract (this is probably the most frequent channel of virus infection) [1]. In the coarse-grained models aimed at the kinetics of viral infection at the level of the susceptible and infected host populations, the transmission is usually described by using the phenomenological mean-field kinetic equations with corresponding rate constants [2,3]. Physicochemical models of the transmission are still lacking except those focused on the pathway (iv) occurring via respiratory droplets generated during sneezing, coughing, and talking. This channel is inherent to viruses, such as influenza and COVID-19, and discussed in more detail in the following paragraphs.

Respiratory droplets are formed of saliva produced and secreted by salivary glands and containing, just after secretion, primarily water ($\simeq$99%) in combination with nonvolatile matter ($\simeq$1%) including sodium, potassium, calcium, magnesium, bicarbonate, phosphates, immunoglobulins, proteins, enzymes, mucins, and nitrogenous products, such as urea and ammonia [4,5]. The fraction of nonvolatile matter in droplets carrying virions can be somewhat higher, up to $\simeq$5% [6]. The size of droplets is often 0.1–20 μm but may be larger [5]. For comparison, spherically shaped lipid-membrane-enveloped COVID-19 virions are $\simeq$100 nm in diameter [7]. The scale of the COVID-19 viral load in saliva is $\sim 10^7$ copies per ml but may be up to $\sim 10^9$ copies per ml [8]. For the droplets with the aforementioned size, the corresponding formally calculated number of virions is $\ll$1. This means that often droplets do not contain virions, and only some of them contain one virion [6]. The distribution of virions in droplets is, however, expected to be far from Poissonian, and some of the droplets, especially large ones, may contain many virions [9].

In air, the coefficient of droplet diffusion and the velocity of the gravity-induced drift are given by the following text-book equations:

$$D = \frac{k_B T}{6\pi\eta R} \quad \text{and} \quad v = \frac{mgD}{k_B T} = \frac{2g\rho R^2}{9\eta}, \tag{1}$$

where R, ρ, and m are the droplet radius, density, and mass ($m = 4\pi\rho R^3/3$), respectively, and η is the air viscosity. To use these equations, one should take into account that the water vapor in the air is often below saturation, and accordingly the droplet size decreases because of evaporation of water. This process is limited by the diffusion of water vapor from the droplet–air interface and to some extent by convection of air near a droplet. For the sizes typical for respiratory droplets, the local convection is usually of minor importance (e.g. Ref. [10]), the evaporation rate calculated per unit area of the droplet–air interface increases with decreasing the droplet size, and the whole evaporation process is fairly fast. In relation to COVID-19, it has recently been confirmed in a few theoretical studies (e.g. Refs. [5,10–12]) using the corresponding textbook models (e.g. Ref. [13]).

At the simplest mean-field level with respect to the interaction of water and nonvolatile matter, the evaporation-related and diffusion-limited decrease of the droplet radius is described as follows [5]:

$$\exp[B\xi(R)]\frac{R}{\chi(R)}\frac{dR}{dt} = -\frac{R^2(0)}{2\tau_e}, \tag{2}$$

where χ and ξ are the volume fractions of water and nonvolatile matter in their mixture, respectively, $B > 0$ is the parameter taking the interaction between water and nonvolatile matter into account, and

$$\tau_e = \frac{R^2(0)}{2v_\circ D_*(c_s - c_\infty)} \tag{3}$$

is the evaporation time scale ($v_\circ$ is volume of a water molecule, D_* is the coefficient of diffusion of water in the gas phase, and c_s and c_∞ are the concentration of water molecules near and far from the interface, respectively).

In general, Eq. (2) should be complemented by the equation describing the evaporation-related decrease of the droplet temperature and the corresponding decrease of c_s. This effect is important but not dramatic. For illustration of the shape of the evaporation kinetics and estimates of the upper value of the evaporation time scale, it can be neglected. In this approximation, Eq. (2)

Figure 1

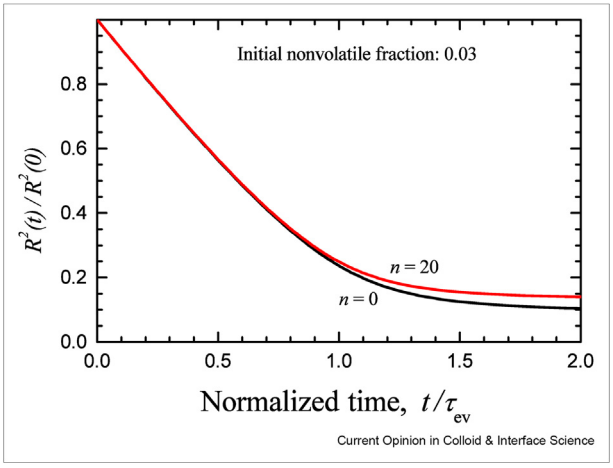

Typical kinetics of evaporation of water from a respiratory droplet. Square of the droplet radius is shown as a function of time for droplets with $R(0)$ = 0.5 μm and dry air (c_∞ = 0). Two curves correspond to the situations with no and 20 virions, respectively. The virion size (diameter) is 100 nm. The results were obtained using Eq. (2) with B = 2 [5].

can be integrated alone (Figure 1). The corresponding kinetics can be divided into two stages. During the main stage, the nonvolatile matter can be neglected, that is, one can set $\chi = 1$ and $\xi = 0$, and Eq. (2) results in the following conventional R^2 law:

$$R^2 = R^2(0)(1 - t/\tau_{ev}). \quad (4)$$

The late stage corresponds to appreciable fraction of the nonvolatile matter in a droplet.

The heat transfer from a droplet to air is described by the equation, which is mathematically similar to the diffusion equation. In general, the joint solution of these equations is complicated by the exponential dependence of c_s on temperature. In the case of respiratory droplets, the variation of temperature is, however, modest, the dependence of c_s on temperature can be linearized, and the main stage of the kinetics can be described analytically [10]. In particular, the R^2 law remains to be valid [10–12]. At a relative humidity of 0.5, the corresponding evaporation time scale for 1-, 5-, and 10-μm-sized droplets is 0.048, 0.12, and 0.48 s, respectively [10].

If the air is stagnant and the size of droplets is constant, their average gravity-induced drift shift and squared diffusion-related displacement are given as follows:

$$\Delta z = mgDt/k_BT \text{ and } \langle \Delta x^2 \rangle + \langle \Delta y^2 \rangle = 4Dt. \quad (5)$$

If m and D depends on time, these equations are modified as follows:

$$\Delta z = \frac{g}{k_BT}\int_0^t m(t')D(t')dt', \ \langle \Delta x^2 \rangle + \langle \Delta y^2 \rangle = 4\int_0^t D(t')dt'.$$

For the main stage of evaporation with the R^2 law, the integrals in these expressions can easily be calculated analytically. According to these expressions, the drift and diffusion-related displacement of respiratory droplets with typical sizes are rather slow [5,10]. Practically, this means that the respiratory droplets move often with air via convection. Various aspects of this motion have recently been analyzed, for example, in Refs. [14–18]. Eventually, the respiratory droplets attach to surfaces. Evaporation of water from droplets located at a surface is described in Refs. [19–21].

In Northern countries, the outdoor air temperature can be below 0 °C. Under such conditions, the temperature inside respiratory droplets rapidly (compared to evaporation) drops below 0 °C as well, droplets become frozen, and then the evaporation is very slow and the motion of frozen droplets is controlled primarily by the gravity (with $m = const$ and $D = const$) and convection.

Taken together, the available models form a good basis for understanding the behavior of respiratory droplets in the air. Additional efforts in this area can be focused, for example, on scrutinizing the specific role of different components of nonvolatile matter on evaporation of water from droplets. In this context, one can notice that the saliva appears to be structured as a highly woven network interconnected by threads [4], and to what extent this feature is important for the transmission of virions is not clear. The available theoretical and experimental data appear to indicate that after evaporation of water from droplets, the nonvolatile matter in its condensed form is protective or at least not too destructive with respect to COVID-19 virions [21].

At the epithelium and in the body

The coarse-grained kinetic models of viral infection are usually temporal and operate with populations of virions and cells inside an infected person [22]. The spatio-temporal models are also available [3,22], but, as already noticed in the Introduction, the mechanistic details of virion transport inside the host are not described explicitly there. In fact, the corresponding full-scale mechanistic models are now often lacking. Although such details can, in principle, be experimentally obtained *in vivo* using optical single-virus tracking techniques, the available studies of this category are limited to investigations of the infection mechanism of viruses in cultured cells [23].

In the case of infections transmitted via air (discussed in the previous section), virions first reach the epithelium. More specifically, virions penetrate a gel-like mobile mucus layer and a brush-like periciliary layer located above the epithelium cells, contact these cells, and then start the viral cycles [24]. The complicating factor here is that the upper gel layer is moving along the cells. The scale of the corresponding velocity is 40 μm/s [25]. The simplest expression for the 2D distribution (concentration) of virions thereafter delivery by a respiratory droplet at $t = 0$ is as follows (cf. Eq (42) in Ref. [5]):

$$c(\mathbf{r},t) = \frac{N_v}{\pi(r_\circ^2 + 4Dt)}\exp\left(-\frac{|\mathbf{r} - \mathbf{v}t|^2}{r_\circ^2 + 4Dt} - (k_p + k_d + k_*)t\right), \quad (6)$$

where N_v is the initial number of virions, $r_\circ$ is the length scale characterizing the initial virion distribution, $\mathbf{v}$ (or v below) is the gel velocity, D is the effective coefficient of virion diffusion in the lumped layer including the mucus

and periciliary layers, and k_p, k_d, and k_* are the virion cell-membrane penetration, detachment, and degradation rate constants, respectively. This expression allows one to classify various possible regimes of the evolution of the initial virion distribution depending on the ratio between the timescales of conversion, $\tau_c = 1/(k_p + k_d + k_*)$, flow-mediated transport, $\tau_c = L/v$, and diffusion, $\tau_d = L^2/4D$ (L is the cell size). More detailed models have recently been proposed in Refs. [25,26]. The spatial distribution of the velocity has been analyzed in Ref. [27].

The spreading of virions in human bodies occurs through blood and lymph vessels and tissue. In the case of COVID-19, for example, the electron microscopy shows virions in endothelial cells across vascular beds of different organs in a series of patients [28]. Theoretically, the transport of virions in blood and lymph vessels can be described by analogy with that of nanoparticles (see the section '**New trends in drug delivery**').

Penetration through a lipid membrane

In Eq. (6), the interaction of virions with the cell membrane is described at the simplest level by introducing the effective penetration rate constant, k_p. In reality, it occurs in a few steps and can be described in more detail. First, a virion associate with a single receptor. This process is expected to be limited by virion diffusion. If the corresponding diffusion coefficient, D [Eq. (1)], is constant and the ligand–receptor tethers are flexible, the association rate constant can be represented as follows [29]:

$$k_{as} = 4\rho D = 4(2l/R)^{1/2}D, \tag{7}$$

where $\rho = (2l/R)^{1/2}$ is the radius of the effective virion-membrane contact area (R is the virion radius, and l is the tether length). A more accurate expression for this rate constant can be obtained taking the slowdown of diffusion near the interface into account [30],

$$k_{as} = 5.9l/D, \tag{8}$$

where D is the diffusion coefficient far from the interface [Eq. (1)]. The subsequent formation of tethers occurs via diffusion of receptors to the virion-cell-membrane contact region as, for example, described in Ref. [31]. This process is accompanied by the membrane bending and then by the virion entry into the cell occurring usually via endocytosis or, in the case of enveloped viruses, via fusion of the virion envelope with the cell membrane (reviewed in Refs. [32,33]). Besides multivalent ligand–receptor interaction and membrane bending, both these processes depend also on the deformation of actin filaments forming the cytoskeleton of the host cell. The models focused on various aspects of viral endocytosis are now numerous (e.g. recent articles [34–38] and references therein).

A virion linked with the lipid membrane by a few tethers can diffuse. This process can be described by various models implying (i) collective diffusion in the 2D lipid fluid [as in the 3D Stokes case (2)] with the logarithmically weak dependence on the number of tethers [39], (ii) nearly independent diffusion of tethers with the diffusion coefficient inversely proportional to the number of tethers [39], or (iii) spider-like diffusion including rupture and formation of tethers [40].

Intracellular viral kinetics

After penetration into the host cells, virions induce host-mediated replication of their RNA or DNA, production of the corresponding proteins, assembly of new virions, and their release to the extracellular environment. Although now some of the intracellular virus-related processes can be directly tracked in cells [41], the understanding of intracellular viral kinetics is still limited. Theoretically, the interplay of the viral replication and the host gene expression is customarily described using a set of temporal mean-field kinetic equations for the intracellular population of various species (reviewed in Ref. [42]). The corresponding models are often generic. The models focused on specific viruses are usually coarse-grained (e.g. Refs. [43,44]; for COVID-19, such models are lacking).

The use of the generic models can be illustrated by referring to the discussion concerning the minimal number of virions needed for the initiation of infection in a host (e.g. Refs. [41,45]). In principle, the infection of one cell by one virion may be sufficient, that is, this number can be as small as one (this is the so-called independent action hypothesis). There are, however, experimental indications that one virion is not sufficient [45]. One of the general ideas here is that in the case of segmented viruses, such as influenza A, a few virions are needed to compensate for intrinsic genetic and/or structural virion defects. The corresponding kinetic model is proposed in Ref. [46].

Another general idea is that a few virions are needed to overcome host infection barriers that limit early viral proliferation, for example, replication [5,45]. More explicitly, this means that (i) in the limit of small number of virions in a cell, the degradation of virions should dominate so that the virion population decreases exponentially provided there is no supply of virions or first grows but then decreases provided the supply of virions is slow and decreases with increasing time down to extinction, and (ii) with increasing number of virions in a cell, their replication should become more efficient due to positive feedback and/or the degradation of virions should become less efficient due to negative feedback [5]. Under such conditions, the stable steady

state corresponds to the extinction of virions. With increasing the number of virions, there is an unstable steady state with transition either back to extinction or to the virion-population growth resulting in the full-scale cell infection. To reach the latter regime, the current number of virions in a cell should be sufficiently large. The corresponding number of the supplied virions should exceed this number and accordingly should be large as well. Mathematically, this can be illustrated using the following simplest coarse-grained equation for the intracellular viral genome population [5]:

$$dN_G/dt = k_r N_G - \kappa_d N_G + w(t), \quad (9)$$

where k_r and κ_d are the replication and degradation rate constants, respectively, and $w(t)$ is the supply rate. The presence of feedback means that these rate constants should depend on N_G. The positive feedback in k_r has already been described [5]. The role of the negative feedback in κ_d can be shown (Figure 2) using the corresponding Hill expression:

$$\kappa_d = \kappa_d^\circ + \kappa_d^* K^m/(K^m + N_G^m), \quad (10)$$

where κ_d°, κ_d^*, K, and m are the corresponding parameters. (The Hill expression is usually used to describe the regulation of gene transcription via protein attachment to the regulatory sites [47]. Here, this expression is used to mimic the feedback in a lumped way without specification of the mechanistic details.)

Intracellular virus-related processes

In the mean-field kinetic models mentioned in the previous section, the elementary steps are characterized by the corresponding rate constants. The mechanistic details of these steps are of high interest. The experimental information concerning the virus-related steps is in fact lacking. On the theoretical side, the mechanisms of the key virus-related steps can, in principle, be described using or by analogy with already available numerous models of the gene expression including transcription of DNA into RNA and RNA translation to proteins (for such models, see, e.g., Refs. [48,49] and references therein). The corresponding theory focused on viruses is now in its initial phase (reviewed in detail in Ref. [50]). One of the processes that has attracted appreciable attention of experimentalists and theoreticians is viral capsid formation (reviewed in Ref. [51]). The corresponding kinetic models are often oriented to academic studies and imply the assembly at steady-state conditions. The model aimed at the assembly *in vivo* under transient conditions was proposed in Ref. [52].

Figure 2

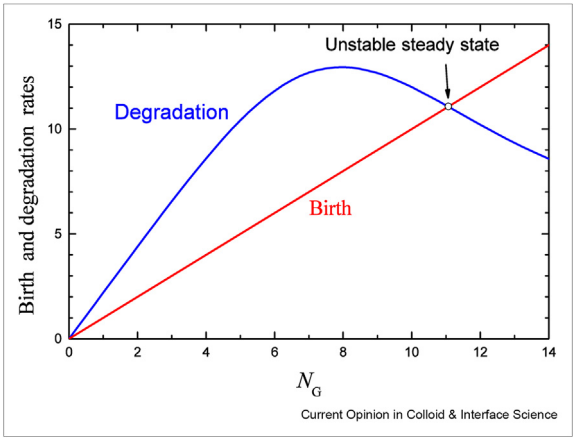

Graphical solution of Eq. (9) with negative feedback for viral genome degradation [Eq. (10) with $\kappa_d^\circ/k_r = 0.2$, $\kappa_d^*/k_r = 2$, $K = 10$, and $m = 4$] and no feedback for replication under steady-state conditions [with $w(t) = 0$]. The virion birth and degradation rates are normalized to k_r.

New trends in drug delivery

CIS is an essential part of the scientific background of pharmaceutics. For example, all disperse systems used in pharmaceutical formulations such as suspensions, emulsions, gels, and ointments include colloid and interface phenomena and their development and optimization are partly based on the CIS approaches [53]. The development of a new generation of drugs is widely expected to be based on advances in CIS and nanoscience. In virology, this implies the use of (i) nanomaterial-enhanced viral replication inhibitors suppressing the production of new virions, (ii) virus-binding nanoparticles including viral membrane inhibitors that can disrupt membrane-enveloped virus particles, (iii) cell membrane decoys binding to virions, and (iv) biomimetic nanoparticle vaccines [54]. In the context of COVID-19, nanoscale vaccine-delivery systems are expected to play a paramount role [55]. For example, two vaccines developed and proved recently by BioNtech and Pfizer and Cambridge-based biotech company include lipid nanoparticles as carriers [56,57]. Nanocarriers of this and other types are now intensively studied in the context of various medical applications [58,59].

The models already developed in CIS or with suitable modifications can be used to rationalize the biophysics related to aforementioned approaches (i)−(iv). In the context of virus-binding nanoparticles (item (ii); see e.g., Ref. [60]), for example, the 3D association of nanoparticles with virions is often limited by diffusion and can be described using the conventional Smoluchowski rate constant, which is as follows:

$$k_a \simeq 4\pi \mathcal{R} D, \quad (11)$$

where $\mathcal{R} = R_1 + R_2$ is the contact radius or, more specifically, the sum of the two nanoparticle radii, and $\mathcal{D}$ is the sum of the diffusion coefficients of the two nanoparticles.

This expression does not take the slowdown of diffusion into account, but this effect is not dramatic in the 3D case [61]. The dissociation rate constant can in turn be represented as follows:

$$k_{\mathrm{d}} \simeq \frac{\mathcal{D}}{l\mathcal{R}[1+\exp(I_{\mathrm{b}}/k_{\mathrm{B}}T)]^{n}}, \tag{12}$$

where $I_{\mathrm{b}} > 0$ and l are the ligand-receptor-pair binding energy and length, respectively, and n is the maximum number of ligand—receptor pairs in the contact area with radius $\rho = [2/R_1R_2/(R_1 + R_2)]$ [cf. with ρ in (7)].

In the context of cell membrane decoys [item (iii)], one is expected to estimate the relative rates of ligand-receptor-pair-mediated association and dissociation of various nanoparticles or their attachment and detachment to membrane receptors. The very initial attachment to membrane receptors has already been discussed briefly [Eqs. (7) and (8)]. The corresponding multivalent aspects of attachment were scrutinized in Refs. [34,62,63].

In all these areas [items (i)-(iii)], the needed selectivity of the species with respect to interaction with virions should be determined under real conditions. Such data are now lacking. This aspect can partly be claried using the CIS-based models.

An important and still poorly understood problem is how to describe drug or vaccine release from nanoparticles [64,65]. The models developed for macroscopic pellets and microcapsules and including conventional Fick's drug diffusion and/or pellet dissolution (see, e.g. Refs. [66,67]) are here not directly applicable because the corresponding mechanistic aspects are different. For example, the delivery of lipid nanoparticles into cells is often followed by their trapping by endosomes, and in this case, the drug or vaccine release is believed to occur through fusion of the lipoplex with the endosome membrane or via transient pores in the endosome membrane [64]. The corresponding fusion- and transient-pore models are conceptual, and their scrutiny is lacking.

Concerning the intracellular kinetics after mRNA delivery and release, I can mention the models presented in Refs. [68,69].

The drug efficiency depends on its distribution in a body after injection. This distribution is often formed via drug convective transport in blood and lymph vessels with subsequent penetration into tissue and diffusion there. The corresponding details are central for optimization of the drug function (in the case of solid tumors, e.g., only ~1% of nanoparticles are now successfully delivered to the target [70], and one of the reasons why this is the case is that nanoparticles often reach and accumulate in lymph nodes and result in toxicity [71]) and also to understand, for example, why drugs tested in mice may fail in human (one of the reasons is the difference in the length and time scales, and this aspect can be clarified using models). This subject is complex due to the abundance of related species and heterogeneity of the systems with a broad distribution of the length and time scales (especially in the case of tumors [72]). The related models including convective and diffusion drug transport and focused often on cancer are numerous and contain many ingredients (see, e.g., recent articles concerning conventional drug delivery [73,74] and delivery by drug-loaded nanocarriers [75,76]). Despite this progress, there is still much room for their improvement.

The type of the model ingredients used in this area can be illustrated by analyzing a generic case of diffusion-controlled drug distribution in the interstitial space around a single cylindrically shaped blood vessel. The corresponding equation for drug concentration is as follows:

$$\frac{\partial c}{\partial t} = \frac{D}{r}\frac{\partial}{\partial r}\left(r\frac{\partial c}{\partial r}\right) - \kappa c, \tag{13}$$

where r is the radial coordinate, D is the diffusion coefficient, and κ is the rate constant associated with the drug consumption by tissue cells. The boundary conditions for this equation near the vessel (at $r = \rho$, where ρ is the vessel radius) can be set as $c(\rho) = c_{\circ}$, where $c_{\circ}$ is the corresponding concentration (it can be equal to that in the vessel if the drug penetration via the vessel wall is rapid or related with that in the vessel, e.g., by analogy with the Starling equation otherwise). The second no-flux boundary condition, $\partial c/\partial r = 0$, can be imposed $r = R$, where R is the distance roughly equal to one half of that up to the adjacent vessels. Physically, the latter no-flux condition separates

Figure 3

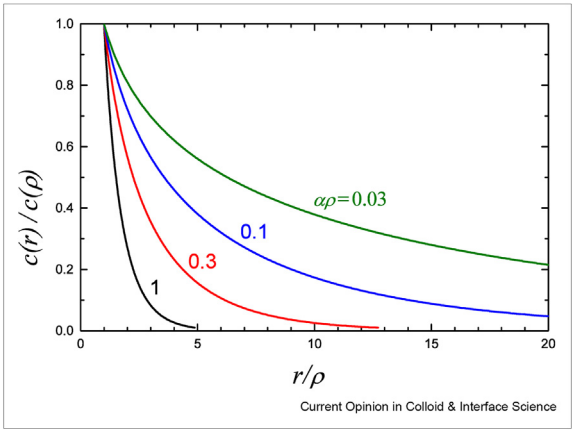

Drug concentration profiles around a cylindrically shaped blood vessel according to Eq. (15) with $\alpha\rho$ = 0.03, 0.1, 0.3, and 1.

the regions associated with different vessels. Taking into account that on the time scale of the drug action, the local drug diffusion is rapid, Eq. (13) can then be solved in the steady-state approximation (by setting $\partial c/\partial t = 0$):

$$c(r) = \frac{K_0(\alpha r)I_1(\alpha R) + I_0(\alpha r)K_1(\alpha R)}{K_0(\alpha \rho)I_1(\alpha R) + I_0(\alpha \rho)K_1(\alpha R)}\, c_\circ, \qquad (14)$$

where $\alpha \equiv (\kappa/D)^{1/2}$, and K_0, I_0, K_1 and I_1 are the modified Bessel functions. If the drug consumption is efficient so that $\alpha R \gg 1$, I_0 in Eq. (14) can be neglected, and we have

$$c(r) = \frac{K_0(\alpha r)}{K_0(\alpha \rho)}\, c_\circ. \qquad (15)$$

This expression predicts that in the practically interesting case with $\alpha\rho \ll 1$, the corresponding concentration profiles are far from exponential (Figure 3). In addition, the drug influx per unit vessel length is weakly dependent on the vessel radius [this follows from the asymptotic expression for $K_0(\alpha r)$] or, in other words, the rate of the drug delivery per unit volume of tissue is roughly inversely proportional to the tissue volume per unit vessel length. The model also shows that even in one of the simplest situations the corresponding equations are relatively complex.

Conclusion

In this brief review, I have outlined various physicochemical models used in virology with a slight bias on those related to COVID-19. Such models are extremely diverse, and from this perspective, the review is far from complete partly because the choice was primarily limited to those linked somehow with CIS. The corresponding links have been indicated explicitly or implied. In general, the interplay between CIS and biology is natural and fruitful. In fact, the focus of studies in CIS is now shifting to different areas of biology, and virology is just one of the examples.

Declaration of competing interest

The author declares that he has no known competing financial interests or personal relationships that could have appeared to influence the work reported in this paper.

Acknowledgments

This work was supported by Ministry of Science and Higher Education of the Russian Federation within the governmental order for Boreskov Institute of Catalysis (project AAAA-A21-121011390008-4).

References

Papers of particular interest, published within the period of review, have been highlighted as:

- • of special interest

1. Cann AJ: *Principles of molecular virology*. Elsevier; 2015.

2. • Bertozzi AL, Franco E, Mohler G, Short MB, Sledge D: **The challenges of modeling and forecasting the spread of COVID-19**. *Proc Nat Acad Sci USA* 2020, **117**:16732–16738.
Example of modeling the spread of COVID-19.

3. Zhdanov VP, Jackman JA: **Analysis of the initiation of viral infection under flow conditions with applications to transmission in feed**. *Biosystems* 2020, **196**:104184.

4. • Sarkar A, Xua F, Lee S: **Human saliva and model saliva at bulk to adsorbed phases - similarities and differences**. *Adv Colloid Interface Sci* 2019, **273**:102034.
Review of the studies of human saliva.

5. • Zhdanov VP, Kasemo B: **Virions and respiratory droplets in air: diffusion, drift, and contact with the epithelium**. *Biosystems* 2020, **198**:104241.
Broad COVID-19-related review focused on virions and respiratory droplets.

6. • Stadnytskyi V, Bax CE, Bax A, Anfinrud P: **The airborne lifetime of small speech droplets and their potential importance in SARS-CoV-2 transmission**. *Proc Nat Acad Sci USA* 2020, **117**:11875–11877.
Experiments concerning evaparoteion of water from respiratory droplets.

7. Zhu N, *et al.*: **A novel coronavirus from patients with pneumonia in China, 2019**. *N Engl J Med* 2020, **382**:727–733.

8. Wölfel R, *et al.*: **Virological assessment of hospitalized patients with COVID-2019**. *Nature* 2020, **581**:465–469.

9. Vejerano EP, Marr LC: **Physico-chemical characteristics of evaporating respiratory fluid droplets**. *J R Soc Interface* 2018, **15**:20170939.

10. • Netz RR: **Mechanisms of airborne infection via evaporating and sedimenting roplets produced by speaking**. *J Phys Chem B* 2020, **124**:7093–7101.
Good analysis of water evaporation from respiratory droplets.

11. Chaudhuri S, Basu S, Kabi P, Unni VR, Saha A: **Modeling the role of respiratory droplets in Covid-19 type pandemics**. *Phys Fluids* 2020, **32**, 063309.

12. Dombrovsky LA, Fedorets AA, Levashov VY, Kryukov AP, Bormashenko E, Nosonovsky M: **Modeling evaporation of water droplets as applied to survival of airborne viruses**. *Atmosphere* 2020, **11**:965.

13. Sazhin S: *Droplets and sprays*. Springer; 2014.

14. Zhang Y, Feng G, Bi Y, Cai Y, Zhang Z, Cao G: **Distribution of droplet aerosols generated by mouth coughing and nose breathing in an air-conditioned room**. *Sustain Cities Soc* 2019, **51**:101721.

15. Busco G, Yang SR, Seo S, Hassan YA: **Sneezing and asymptomatic virus transmission**. *Phys Fluids* 2020, **32**, 073309.

16. Dbouk T, Drikakis D: **On coughing and airborne droplet transmission to humans**. *Phys Fluids* 2020, **32**, 053310.

17. Pendar M-R, Pascoa JC: **Numerical modeling of the distribution of virus carrying saliva droplets during sneeze and cough**. *Phys Fluids* 2020, **32**, 083305.

18. Wang B, Wu H, Wan X-F: **Transport and fate of human expiratory droplets - a modeling approach**. *Phys Fluids* 2020, **32**, 083307.

19. Bhardwaj R, Agrawal A: **Likelihood of survival of coronavirus in a respiratory droplet deposited on a solid surface**. *Phys Fluids* 2020, **32**, 061704.

20. Bhardwaj R, Agrawal A: **Tailoring surface wettability to reduce chances of infection of COVID-19 by a respiratory droplet and to improve the effectiveness of personal protection equipment**. *Phys Fluids* 2020, **32**, 081702.

21. • Bhardwaj R, Agrawal A: **How coronavirus survives for days on surfaces**. *Phys Fluids* 2020, **32**:111706.
Discusion of the role of the nonvolatile matter in carrying COVID 19 virions by respiratory droplets.

22. • Handel A, La Gruta NL, Thomas PG: **Simulation modelling for immunologists**. *Nat Rev Immunol* 2020, **20**:186–195.

Review of the kinetic models of viral infections.

23. Liu S-L, Wang Z-G, Xie H-Y, Liu A-A, Lamb DC, Pang D-W: **Single-virus tracking: from maging methodologies to virological applications**. *Chem Rev* 2020, **120**:1936–1979.

24. de Vries E, Du W, Guo H, de Haan CAM: **Influenza A virus hemagglutinin-neuraminidase-receptor balance: preserving virus motility**. *Trends Microbiol* 2020, **28**:57–67.

25. Quirouette C, Younis NP, Reddy MB, Beauchemin CAA: **A mathematical model describing the localization and spread of influenza A virus infection within the human respiratory tract**. *PLoS Comput Biol* 2020, **16**, e1007705.

26. Whitman J, Dhanji A, Hayot F, Sealfon SC, Jayaprakash C: **Spatio-temporal dynamics of host-virus competition: a model study of influenza A**. *J Theor Biol* 2020, **484**:110026.

27. Shang Y, Inthavong K, Tu J: **Development of a computational fluid dynamics model for mucociliary clearance in the nasal cavity**. *J Biomech* 2019, **85**:74–83.

28. Varga Z, *et al.*: **Endothelial cell infection and endotheliitis in COVID-19**. *Lancet* 2020, **395**:1417–1418.

29. Zhdanov VP, Höök F: **Diffusion-limited attachment of large spherical particles to flexible membrane-immobilized receptors**. *Eur Biophys J* 2015, **44**:219–226.

30. • Zhdanov VP: **Diffusion-limited attachment of nanoparticles to flexible membrane-immobilized receptors**. *Chem Phys Lett* 2016, **649**:60–63.
Analysis of the effect of non-ideality of diffusion near an interface on the attachment.

31. Gibbons MM, Chou T, D'Orsogna MR: **Diffusion-dependent mechanisms of receptor engagement and viral entry**. *J Phys Chem B* 2010, **114**:15403–15412.

32. Helenius A: **Virus entry: looking back and moving forward**. *J Mol Biol* 2018, **430**:1853–1862.

33. García IL, Marshb M: **A biophysical perspective on receptor-mediated virus entry with a focus on HIV**. *BBA - Biomembr* 2020:1862. 183158.

34. • Zhdanov VP: **Kinetics of virus entry by endocytosis**. *Phys Rev E* 2015, **91**, 042715.
Model of the viral entry into cells.

35. Banerjee A, Berezhkovskii A, Nossal R: **Kinetics of cellular uptake of viruses and nanoparticles via clathrinmediated endocytosis**. *Phys Biol* 2016, **13**, 016005.

36. Hassinger JE, Oster G, Drubin DG, Rangamani P: **Design principles for robust vesiculation in clathrin-mediated endocytosis**. *Proc Natl Acad Sci USA* 2017, **114**:E1118–E1127.

37. Bai F, Wu J, Sun R: **An investigation of endocytosis of targeted nanoparticles in a shear flow by a statistical approach**. *Math Biosci* 2018, **295**:55–61.

38. Di Michele L, Jana PK, Mognetti BM: **Steric interactions between mobile ligands facilitate complete wrapping in passive endocytosis**. *Phys Rev E* 2018, **98**, 032406.

39. • Block S: **Brownian motion at lipid membranes: a comparison of hydrodynamic models describing and experiments quantifying diffusion within lipid bilayers**. *Biomolecules* 2018, **8**:30.
Discussion of diffusion of nanoparticles linked to a lipid bilayer.

40. Hamming PH, Overeem NJ, Huskens J: **Influenza as a molecular walker**. *Chem Sci* 2020, **11**:27–36.

41. • Rocha S, Hendrix J, Borrenberghs D, Debyser Z, Hofkens J: **Imaging the replication of single viruses: lessons learned from HIV and future challenges to overcome**. *ACS Nano* 2020, **14**:10775–10783.
Review of the advances in the studies of viruses in cells.

42. • Yin J, Redovich J: **Kinetic modeling of virus growth in cells**. *Microbiol Mol Biol Rev* 2018, **82**. e00066-17.
Review of the models of intracellular viral kinetics.

43. Handel A, Liao LE, Beauchemin CAA: **Progress and trends in mathematical modelling of influenza A virus infections**. *Curr Opin Syst Biol* 2018, **12**:30–36.

44. Goyal A, Liao E, Perelson AS: **Within-host mathematical models of hepatitis B virus infection: past, present, and future**. *Curr Opin Syst Biol* 2019, **18**:27–35.

45. • **Sanjuán R: collective properties of viral infectivity**. *Curr Opin Virol* 2018, **33**:1–6.
Discussion of the independent action hypothesis.

46. Segredo-Otero E: **Sanjuán R: The effect of genetic complementation on the fitness and diversity of viruses spreading as collective infectious units**. *Virus Res* 2019, **267**:41–48.

47. Zhdanov VP: **Kinetic models of gene expression including non-coding RNAs**. *Phys Rep* 2011, **500**:1–42.

48. Cao Z, Filatova T, Oyarzun DA, Grima R: **A Stochastic model of gene expression with polymerase recruitment and pause release**. *Biophys J* 2020, **119**:1002–1014.

49. Szavits-Nossan J, Evans MR: **Dynamics of ribosomes in mRNA translation under steady- and nonsteady-state conditions**. *Phys Rev E* 2020, **101**, 062404.

50. Altan-Bonnet G, Mora T, Walczak AM: **Quantitative immunology for physicists**. *Phys Rep* 2020, **849**:1–83.

51. Zandi R, Dragnea B, Travesset A, Podgornik R: **On virus growth and form**. *Phys Rep* 2020, **847**:1–102.

52. • Zhdanov VP: **Viral capsids: kinetics of assembly under transient conditions and kinetics of disassembly**. *Phys Rev* 2014, **90**, 042721.
Model of the intracellular viral-capsid formation.

53. Tadros T: **Colloid and interface aspects of pharmaceutical science**. In *Colloid and interface science in pharmaceutical research and development*. Edited by Ohshima H, Makino M, Elsevier; 2014:29–54.

54. • Jackman JA, *et al.*: **Biomimetic nanomaterial strategies for virus targeting: antiviral therapies and vaccines**. *Adv Funct Mater* 2020:2008352.
Discussion of the new trends in virology.

55. Florindo HF, *et al.*: **Immune-mediated approaches against COVID-19**. *Nat Nanotechnol* 2020, **15**:630–645.

56. **Nanomedicine and the COVID-19 vaccines (editorial)**. *Nat Nanotechnol* 2020, **15**:963.

57. Jeyanathan M, Afkhami S, Smaill F, Miller MS, Lichty BD, Xing Z: **Immunological considerations for COVID-19 vaccine strategies**. *Nat Rev Immunol* 2020, **20**:615–632.

58. • Mitchell MJ, Billingsley MM, Haley RM, Wechsler ME, Peppas NA, Langer R: **Engineering precision nanoparticles for drug delivery**. *Nat Rev Drug Discov* 2021, **20**:101–124.
Good review of the use of nanoparticles for drug delivery.

59. Li B, Zhang X, Dong Y: **Nanoscale platforms for messenger RNA delivery**. *WIREs Nanomed Nanobiotechnol* 2019, **11**, e1530.

60. Wallert M, *et al.*: **Mucin-inspired, high molecular weight virus binding inhibitors show biphasic binding behavior to influenza A viruses**. *Small* 2020, **16**:2004635.

61. Zhdanov VP: **Note: the effect of viscosity on the rate of diffusion-limited association of nanoparticles**. *J Chem Phys* 2015, **143**:166102.

62. • Zhdanov VP: **Multivalent ligand-receptor-mediated interaction of small filled vesicles with a cellular membrane**. *Phys Rev E* 2017, **96**, 012408.
Discusion of the kinetic aspects of multivalent interaction.

63. • Liu M, *et al.*: **Combinatorial entropy behaviour leads to range selective binding in ligand-receptor interactions**. *Nat Commun* 2020, **11**:4836.
Discusion of the kinetic aspects of multivalent interaction.

64. • Degors IMS, Wang C, Rehman ZU, Zuhorn IS: **Carriers break barriers in drug delivery: endocytosis and endosomal escape of gene delivery vectors**. *Acc Chem Res* 2019, **52**: 1750–1760.
Review of major biological barriers that are confronted by nanotherapeutics.

65. • Zhdanov VP: **Intracellular RNA delivery by lipid nanoparticles: diffusion, degradation, and release**. *Biosystems* 2019, **185**: 104032.
Discusion of the kinetic aspects of the function of lipid nanoparticles.

66. Siepmanna J, Siepmann F: **Mathematical modeling of drug dissolution**. *Intern J Pharm* 2013, **453**:12–24.

67. Carr EJ, Pontrelli G: **Drug delivery from microcapsules: how can we estimate the release time?** *Math Biosci* 2019, **315**: 108216.

68. Zhdanov VP: **Kinetics of lipid-nanoparticle-mediated intracellular mRNA delivery and function**. *Phys Rev E* 2017, **96**, 042406.

69. Zhdanov VP: **mRNA function after intracellular delivery and releaseVladimir**. *Biosystems* 2018, **165**:52–56.

70. Ouyang B, *et al.*: **The dose threshold for nanoparticle tumour delivery**. *Nat Mater* 2020, **19**:1362–1371.

71. Dukhin SS, Labib ME: **Convective diffusion of nanoparticles from the epithelial barrier toward regional lymph nodes**. *Adv Colloid Interface Sci* 2013, **199–200**:23–43.

72. Dewhirst MW, Secomb TW: **Transport of drugs from blood vessels to tumour tissue**. *Nat Rev Canc* 2017, **17**:738–750.

73. • d'Esposito A, *et al.*: **Computational fluid dynamics with imaging of cleared tissue and of in vivo perfusion predicts drug uptake and treatment responses in tumours**. *Nature Biomed Eng* 2018, **2**:773–787.
Standards of the models of drug uptake in tumours.

74. Moradi Kashkooli F, Soltani M, Hamedia M-A: **Drug delivery to solid tumors with heterogeneous microvascular networks: novel insights from image-based numerical modeling**. *Europ J Pharm Sci* 2020, **151**:105399.

75. • Lane LA: **Physics in nanomedicine: phenomena governing the *in vivo* performance of nanoparticles**. *Appl Phys Rev* 2020, **7**, 011316.
Review of the models of nano-sized-drug delivery to tumors.

76. Moradi Kashkooli F, Soltani M, Souri M, Meaney C, Kohandel M: **Nexus between *in silico* and *in vivo* models to enhance clinical translation of nanomedicine**. *Nano Today* 2021, **36**: 101057.